Supplement of Atmos. Meas. Tech., 16, 5205–5215, 2023
https://doi.org/10.5194/amt-16-5205-2023-supplement

Atmospheric Measurement Techniques
Open Access
EGU

Supplement of

The viscosity and surface tension of supercooled levitated droplets determined by excitation of shape oscillations

Mohit Singh et al.

Correspondence to: Denis Duft (denis.duft@kit.edu)

1. EDB setup description

The geometrical construction of the ElectroDynamic Balance (EDB) includes one hyperboloidal torus electrode having an internal radius of r_0=5 mm and two hyperboloidal end cap electrodes placed on the top and bottom of the torus electrode. An Alternating Current (AC) potential of 1.7 kV with a frequency of between 150 Hz to 500 Hz is applied to the torus electrode and serves as the potential for droplet levitation. A static Direct Current (DC) potential is applied to the endcap electrodes to compensate for the gravitational force acting on the droplet. Individual charged liquid droplets are generated by a droplet injector containing a driven drop-on-demand piezo generator (GeSiM). Droplets are charged by induction in the moment of droplet formation by applying a high voltage DC potential close to the tip of the injector nozzle. Using this particular injector type, droplets of diameter ~100 µm carrying a charge of 0.3 pC to 3 pC are reproducibly injected and levitated in the EDB. A resistive heating element is mounted onto the generator to decrease viscosity and prevent freezing of the liquid at the end of the nozzle at low temperatures. The temperature of the EDB is adjusted using a chiller (Julabo FP50-HE) connected to the cooling circuit attached to the central torus electrode. Both endcap electrodes are mounted onto the torus electrode using an electrically insulating material as a spacer which allows high thermal conductivity at the same time. The temperature inside the EDB can be adjusted between 303 K and 233 K with ±0.5 K accuracy. A HeNe laser (632.8 nm, JDS Uniphase) polarized parallel to the scattering plane, is directed on to the levitated droplet through optical ports in the chamber and EDB body and the scattered light is analysed via several optical ports for different purposes. Light scattered through one port is focused onto a vertically oriented CCD-line detector providing a direct measurement for the vertical droplet position. The information of the vertical position is used for two purposes: (1) automatic adjustment of the DC potential in order to compensate the gravitational force and position the droplet in the centre of the EDB, and (2) to adjust the AC levitation frequency to ensure stable trapping of the levitated droplet. A second optical port in the chamber body located at 90° to the incoming laser beam is used to probe the scattered light over an angular range of 18.7°. The scattered light is directed to a 50:50 beam splitter. One path is used to obtain angular resolved scattering images which are recorded using a CCD camera. These images are subsequently analysed and compared with Mie scattering theory to determine the droplet size. The other path is used to focus the scattered light on to a photomultiplier tube (PMT) (Hamamatsu H10723-20, frequency bandwidth (-3 dB) = 200 kHz) to record the scattered light intensity with much higher time resolution than the CCD camera. The analog output signal of the PMT and the reference signal are recorded simultaneously with a digitizer (National Instruments, NI 9223) at a 1 MHz sample rate. One optical port of the EDB remains unused.

2. High frequency (HF) AC signal generator

In order to probe the natural frequency of shape oscillations of a charged droplet levitated in an EDB, two AC frequencies are required: a low frequency AC applied to the torus electrode for stable droplet levitation (~150-500 Hz), and a high frequency AC applied to the endcap electrodes to excite the shape oscillations (~9 k-40 kHz). Figure S1 shows a schematic of the custom-built high-frequency generator. The generator consists of the following parts: 1) a low-voltage sine-wave generator whose frequency can be set digitally e.g., via interface to a PC and

whose output is used as an input for a variable gain operational amplifier (OP-AMP). The output of the OP-AMP is used to drive two identical ferrite core transformers (T1 and T2) connected in parallel. The amplitude of the AC-output can be varied by adjusting the gain of the OP-AMP.

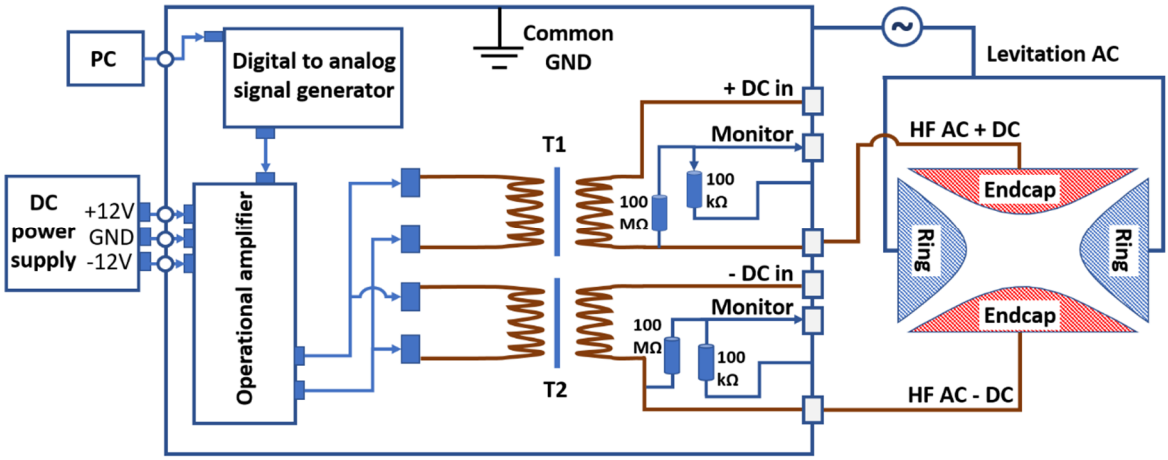

Figure S1 *Schematic of the custom HF-AC signal generator.*

To maximize the AC-output amplitude, the primary-to-secondary winding ratio of the transformers is carefully selected to achieve a transformer resonance at 19 kHz, slightly above the range of natural droplet oscillation frequencies which we anticipated to occur between 13 and 17 kHz. One end of the secondary winding of each transformer is connected to the DC inputs, and the other end is connected to the end cap electrodes of the EDB. This ensures that the DC component is independent of the amplitude of the AC-excitation potential. The HF generator can produce up to 2 kV peak-to-peak (pp) voltage with a variable frequency of 1-50 kHz. In the experiments, however, the HF generator output was kept at a maximum of 1.5 kVpp in order to avoid electrical discharges in the EDB. To address the nonlinearity in the transformer output, the operational amplifier was programmed accordingly. This programming allowed for maintaining a constant output amplitude to be upheld across the entire frequency spectrum. The outputs of both transformers are connected to a 1:1000 voltage divider in order to provide low-voltage reference signals. The reference signals are connected to an oscilloscope and to the digitizer for continuous monitoring of the output HF AC signal. Naturally, a frequency-dependent phase shift occurs between the input and output of a transformer. Both transformers are in fact not fully identical but differ slightly in their resonance frequency and peak amplitude. As a consequence, both output AC signals exhibit a slightly different frequency-dependent phase shift with respect to the input sine signal from the OP-AMP. Far from the transformer resonance frequency e.g., at 10 kHz, this phase shift difference between the transformer outputs is on the order of 1°. In the vicinity of the transformer resonance frequency the phase shift difference is most pronounced and can amount to several degrees. Having a frequency-dependent phase difference between the AC potentials on the top and the bottom endcap electrode is not ideal and has led to deviations in the determined phase shifts when droplet and transformer Eigenfrequencies coincide. Therefore, the phase shift was not probed in a frequency range between 17 and 21 kHz around the transformer resonance peak (c.f. Fig. 4 in the manuscript). This part of the setup is subject to change in the future for an improved version of the setup.

3. Size measurement

Droplet sizing techniques using light scattering have been reviewed recently by Davies (2019). Here, we follow an approach similar to the one described by Steiner et al. (1999) which is based on determining the droplet size by analysing the frequency of fringes appearing in light scattering images of the droplet. A continuous series of light scattering images at 1 s time intervals is recorded using the CCD camera while the droplet is levitated in the EDB.

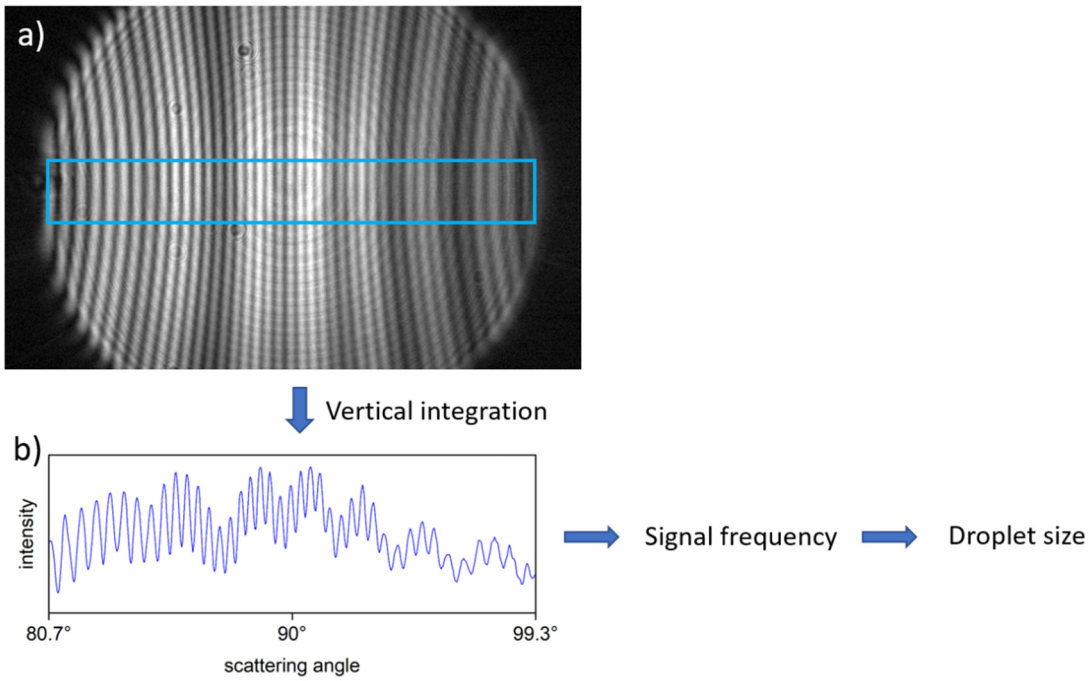

Figure S2 *Steps for retrieving the droplet size from recorded light scattering images. Panel a) Light scattering image of a single droplet. Panel b) Phase function obtained by integrating the boxed area shown in panel a) in the vertical direction.*

Panel a) in Fig. S2 shows a recorded light scattering image around the 90° scattering angle. The scattered light is integrated within the boxed region in the vertical direction to improve the signal to noise ratio. The resulting intensity as a function of scattering angle is called the phase function and displayed in panel b) of Fig. S2. The droplet size is determined by analysing the spatial frequency of fringes in the phase function, given that refractive index, scattering angle and polarization of the recorded scattered light are known.

Panel b) in Fig. S2 shows the phase function corresponding to the scattering image above. It is clear that a Fourier analysis of this phase function would reveal the presence of several frequency components. In certain cases, this approach can lead to ambiguity in identifying the primary spatial frequency. Therefore, we filter the series of light scattering images, by selecting only those where the primary peak frequency can unambiguously be identified. From the remaining light scattering images, the spatial frequency of fringes is determined. Using the spatial frequency, the droplet size is determined by comparison with a library of spatial frequencies generated using Mie theory as a function of size and refractive index.

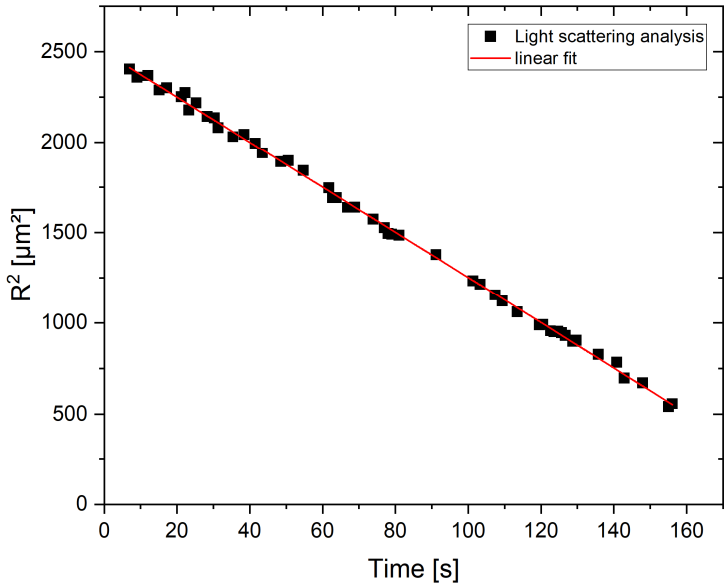

Figure S3 *Square of the radius of an evaporating water droplet at T=0.2°C as function of time plotted together with a linear fit of the data. The fit yielding R_0=50µm and b=12.48µm²s^{-1}.*

The analysis procedure described above is applied in an automated fashion to all light scattering images. As described above, images with phase functions that exhibit ambiguous spatial frequencies are excluded and the droplet radius is determined for the remaining images. This results in a time series for the droplet radius. An example result of such an analysis for a water droplet at 0.2 °C is shown in Fig. S3 where the square of the droplet radius versus time is plotted. The gaps in the series of data point are a result of the image filtering procedure. The droplet evaporation rate is calculated by fitting a straight line to the data according to the equation $R^2(t) = R_0^2 - b \cdot t$ where R_0 is the radius at time t = 0 and b is the evaporation rate coefficient. The scatter in the data points is a result of a small remaining ambiguity in determining the spatial frequency in the phase functions and is of a statistical nature. As a result, the fitted equation provides a significantly more accurate representation of the droplet radius as function of time. Measuring droplet size using single non pre-selected images, we estimate a relative uncertainty in size of 4 %. Using the fitted equation as a representation for the droplet size reduces this uncertainty substantially to about 1 %.

4. Charge measurement

The vertical position control feature of the experiment keeps the droplets in the centre of the EDB at all times. This means that the gravitational force acting on the droplet is always balanced by the vertical static electric DC field. The mass-to-charge ratio of the droplet can be directly calculated from the applied DC potential by equating gravitational and electrical forces. This yields for the mass-to-charge ratio:

$$\frac{m}{Q} = \frac{U}{gd} \cdot C_0 \qquad \text{(E1)}$$

where g is the gravitational acceleration, U is the DC potential difference, $d = \sqrt{2} \cdot 5mm$ is the distance between the endcap electrodes to which the DC is applied, and $C_0 = 0.767$ is the geometry constant representative for the electrode arrangement.

Knowing the radius and the density of the droplet, the mass-to-charge ratio can be used to calculate the droplet charge. This is shown for a single evaporating water droplet in Fig. S4. The spike at about 6 s marks the moment when the droplet is injected into the EDB. The droplet charge remains constant as is expected as only neutral molecules evaporate from the droplet surface. If the vertical position control is not adjusted ideally this will show as an apparent deviation of the particle charge from the constant value as can be seen to occur also in this example after about 70 s. However, the constant part of the time series is enough to determine the droplet charge. We estimated the relative uncertainty in droplet charge measurement to be about 3.5 %.

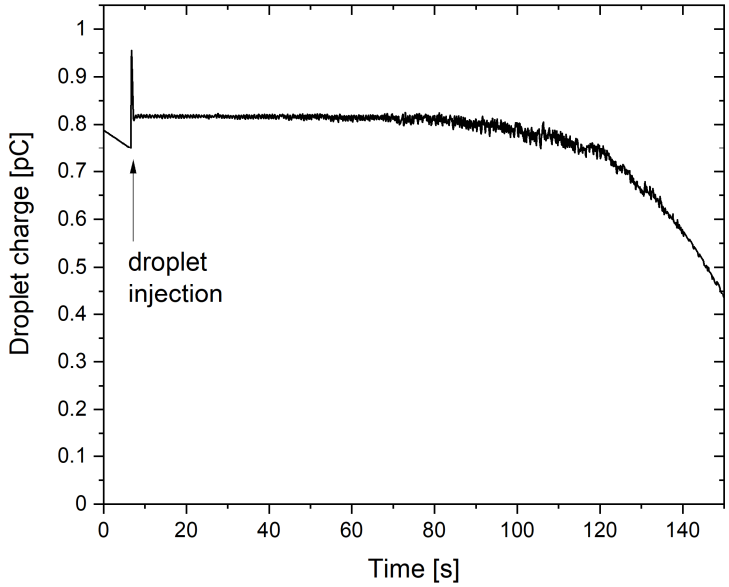

Figure S4 *Calculated droplet charge as function of time of the levitated water droplet shown in Fig. S3.*

The uncertainties for the viscosity and surface tension are all calculated according to error propagation based on the equations in the manuscript. As the measurement of viscosity and surface tension strongly depends on the droplet size, improving the size determination method would provide great benefit to a future revised setup.

5. Cycle symmetry method – a method for the analysis of phase shift between excitation and response

A charged droplet levitated in the EDB constitutes a forced harmonic oscillator whose shape oscillations are driven by the alternating field of the levitator. The analysis of such a system of periodic excitation and harmonic response is often performed using the phase-sensitive detection or lock-in technique which yields the amplitude of the forced oscillation and the phase shift between excitation and response. The phase shift can be used to calculate the restoring force constant as well as the damping constant of the system. The lock-in method can be effective in many linear systems where signal and noise can be adequately separated. The method may not work optimally in highly non-linear systems. The intensity of light scattered by a spherical droplet under a selected angular range is a highly non-linear function of droplet size and shape rendering lock-in analysis more error-prone. We therefore apply an alternative method for analysing the light scattered by the oscillating droplets. In the following we will

show some fundamental properties of the light scattered by oscillating droplets and how this can be used to determine the phase shift between excitation and droplet response.

5.1 Light scattering from oscillating droplets

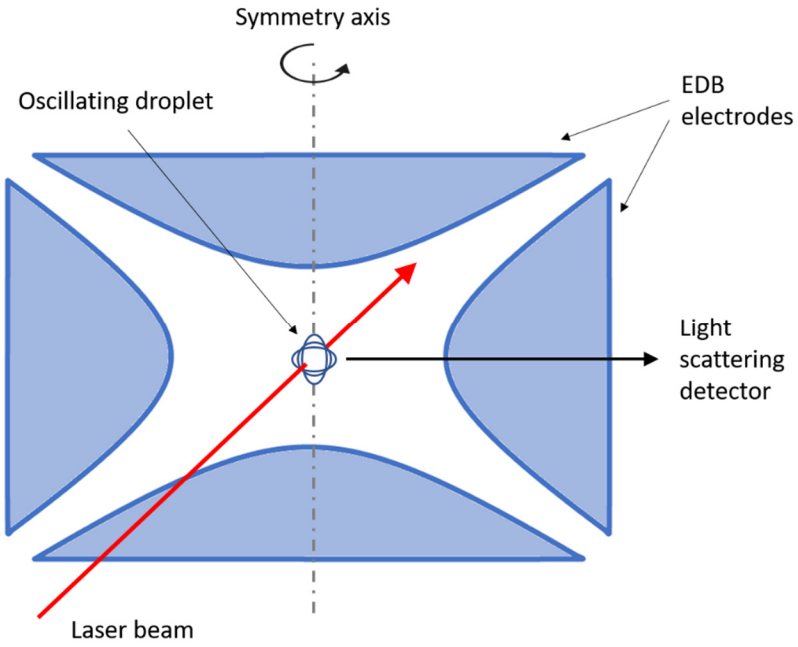

Figure S5 *Simplified vertical cross section of the EDB and the optical geometry for recording the light scattered by a shape-oscillating droplet. The size of the droplet and the amplitude of the shape oscillation are grossly exaggerated. As a reference, typical droplet diameter is about 100 µm while shape oscillations with an amplitude as low as 0.4 nm can be detected.*

The alternating electric field of a 3D quadrupole ion trap drives shape oscillations of the charged droplet levitated in the centre of the ion trap (Fig. S5). For not too large of an oscillation amplitude, the droplet shape can be approximated by a rotational symmetric ellipsoid. Figure S6 shows three phases of the ellipsoidal droplet deformation oscillating between prolate (left), spherical (centre), and oblate (right). In order to facilitate analysis of the complex Mie-scattering pattern as a result of the changing droplet shape, we will apply the equator model (Duft, 2011).

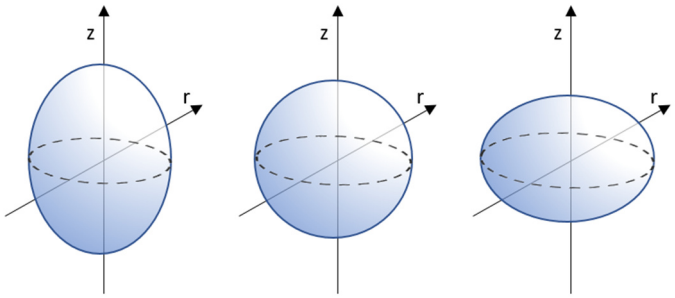

Figure S6 *Schematic of the equator model for an oscillating droplet. In the equator model the light scattered perpendicular to the symmetry axis by an ellipsoid can be approximated by the light scattered by a sphere with equivalent equatorial radius (dashed lines).*

The equator model states, that if the light source and the light scattering detector are placed within the equatorial plane of the ellipsoidal droplet, then the detected light scattering signal of the ellipsoid can be approximated by the light scattered by a sphere with equivalent equatorial radius. This equator or equivalent-sphere model reduces the computational effort of calculating the scattered light significantly as existing numerical code for Mie-scattering of spheres is readily available. It was shown that this approximation gives very good results, as long as the forming ellipse of the ellipsoid is within the aspect ratio (AR) range of 0.97<AR<1.03 which translates to a maximum eccentricity, e of the forming ellipse of about e=0.24 (Duft, 2011). The equator model was shown to be valid for the exemplary case of a water droplet (n=1.333) of diameter D=20 µm and laser wavelength of 632.8 nm. If the oscillation amplitude is kept within this aspect ratio range, then the light recorded by the detector placed perpendicular to the axis of rotation of the quadrupole field can be approximated by the light scattered by a sphere with a periodically changing radius.

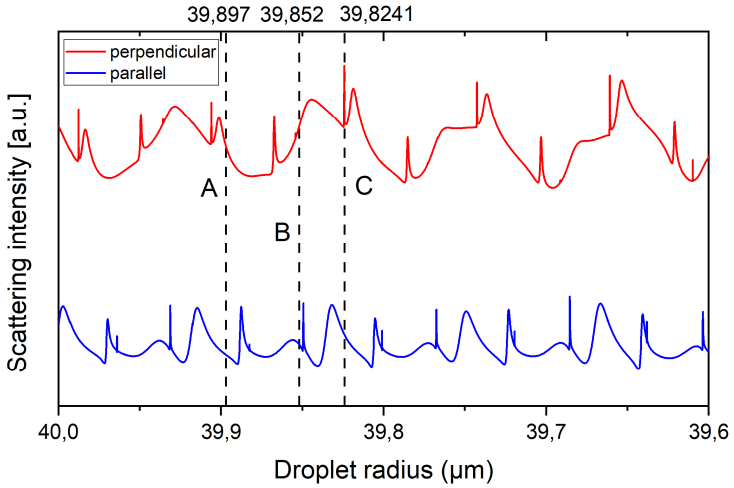

Figure S7 *Light scattered by a spherical water droplet, calculated using Mie-theory. Scattered intensity is integrated over the scattering angle range between 80-100°.*

Figure S7 shows the light scattered according to Mie-theory for a spherical droplet as a function of droplet radius in the narrow radius range between 39.6 µm and 40 µm, split into its components polarized perpendicular and parallel to the scattering plane. For this example, a water droplet (refractive index n=1.333) was chosen and the scattered light was integrated between 80° and 100° of the scattering angle. The figure shows that both polarizations are characterized by quasi-periodic appearance of peaks of varying sharpness whose origin are the so-called morphology dependent resonances (MDR) (Bohren and Huffman, 2008).

Applying the equator model and Mie theory for spherical particles, we immediately can derive a theoretical time dependent light scattering signal received from the oscillating droplet. The result is shown in Fig. S8 for three different droplets with slightly different spherical droplet radii and otherwise identical properties as indicated by labels A, B, and C in Fig. S7. All three droplets oscillate with their equivalent-sphere radius around the spherical radius. The light scattering signal resulting from a very small oscillation amplitude of 0.4 nm (4 Å!) and a phase shift of 0° is shown in the lower panel of Fig. S8, while in the upper panel the reference input signal is shown for comparison.

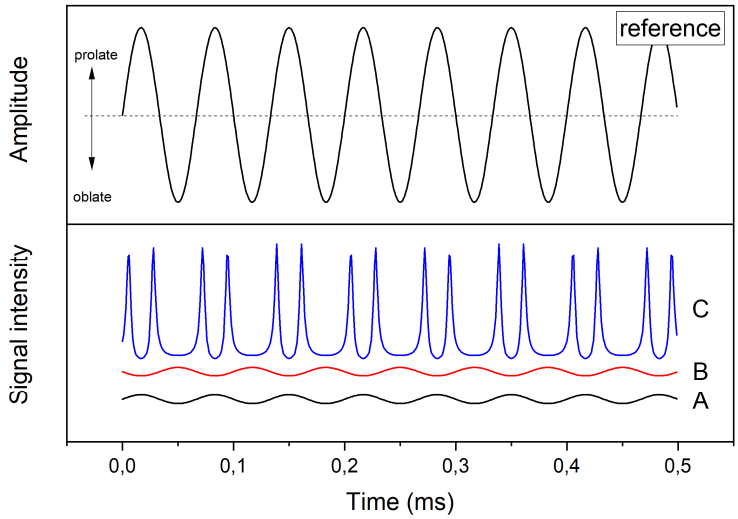

Figure S8 *Calculated intensity of scattered light (lower panel) for an oscillating droplet for three different radii as indicated by the three vertical lines in Fig. S7. The amplitude of oscillation is 0.4 nm. The reference input signal is shown in the upper panel.*

Two main observations can be made from Fig. S8:

1. Even though the phase of the excitation is the same for all three droplets, the optical response of the scattered light can vary from apparently being in phase with the input driving force (case A) to being 180° out of phase (case B) to cases with unclear phase relation (case C).
2. The signal intensity varies greatly depending on the sharpness of the MDR the droplet size is centred at (see Fig. S7).

A consequence of observation (1) is that the lock-in method may give inconsistent results for such a system. Therefore, an alternative method, the cycle symmetry method, was developed to determine the phase relation between the input signal and droplet response.

5.2 The cycle symmetry method

The proposed method relies on the idea that, independent of the characteristics of the light scattering time series data, the signal in principle always retains the symmetry with respect to the extrema of the actual oscillation (as long as the oscillation remains harmonic). The goal was hence to find a method of analysing the signal symmetry in relation to the phase of the input reference.

To obtain a measure for the symmetry of our signal we use the property that any real function can be written as the sum of an even (symmetric) and an odd (antisymmetric) part. This can also be applied to a sequence of measured data as long as the measurement is performed in equidistant steps of the independent variable. Within a window of 2N+1 data points we decompose the signal (x_i) into its even (e_i) and odd (o_i) components with respect to the window's central point x_n according to

$$e_i = \frac{1}{2}(x_{n-i} + x_{n+i}), i = -N \dots N \qquad \text{E2)}$$

$$o_i = \frac{1}{2}(x_{n-i} - x_{n+i}),\ i = -N \ldots N \qquad \text{E3)}$$

such that the original signal can be recovered by adding e_i and o_i. In practice, it is sufficient to calculate only the even component. As a scalar measure for the symmetry of the signal with respect to point x_n we use the normalized even energy E_n:

$$E_n = \frac{2\sum_{i=0}^{N} e_i^2}{\sum_{i=-N}^{N} x_i^2} \qquad \text{E4)}$$

Sliding the window of 2N+1 points along the signal gives a scalar value for the even energy for each time step t_n of the signal time series, or phase of the reference input, respectively.

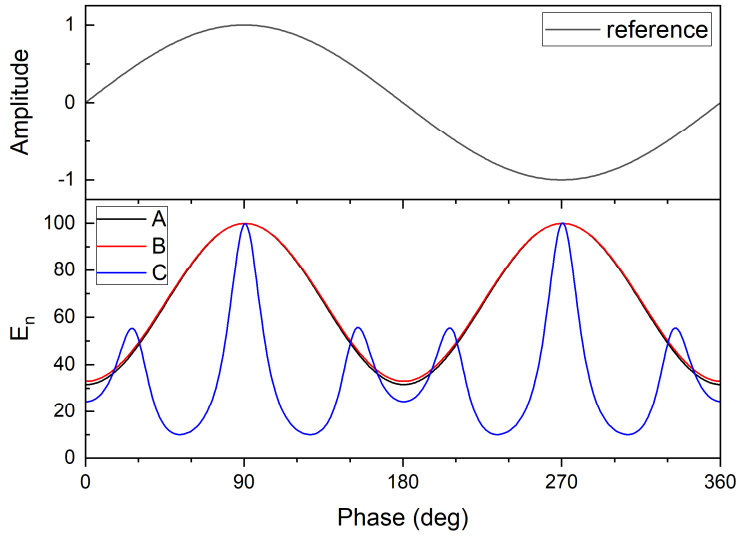

Figure S9 *Cycle symmetry analysis. Upper panel: amplitude of reference signal. Lower panel: Symmetry profiles determined using even energy (eq. E4) of output sequences (cases A, B and C from Fig. S8) with respect to the reference phase.*

Figure S9 shows the calculated even energy of the signal for the three cases A-C depicted in Fig. S8 as function of the phase of the input reference. The window size was chosen to have a length corresponding to one period of the reference input frequency. The maxima of the symmetry profiles indicate the points of highest symmetry which we identify as the turning points of the droplet oscillation, i.e. the points of maximum prolate and oblate deformation. Using a one-period sliding window, the phase shift between input and response can be retrieved by recording and analysing the signal over two periods of the reference only. The method is tolerant to some degree of noise within the signal output. Signal noise, however, will influence the accuracy of the measured phase from single cycles. This can be improved by averaging the symmetry profiles over a number of consecutive cycles as detailed below.

5.3 Performance

To compare the performance of both methods for highly variable output signals such as the intensity of light scattered by an oscillating droplet surface, experimental data was collected for a Lithium Chloride solution droplet levitated in the electrodynamic balance and excited by a superimposed harmonic potential with a frequency between 10 and 15 kHz.

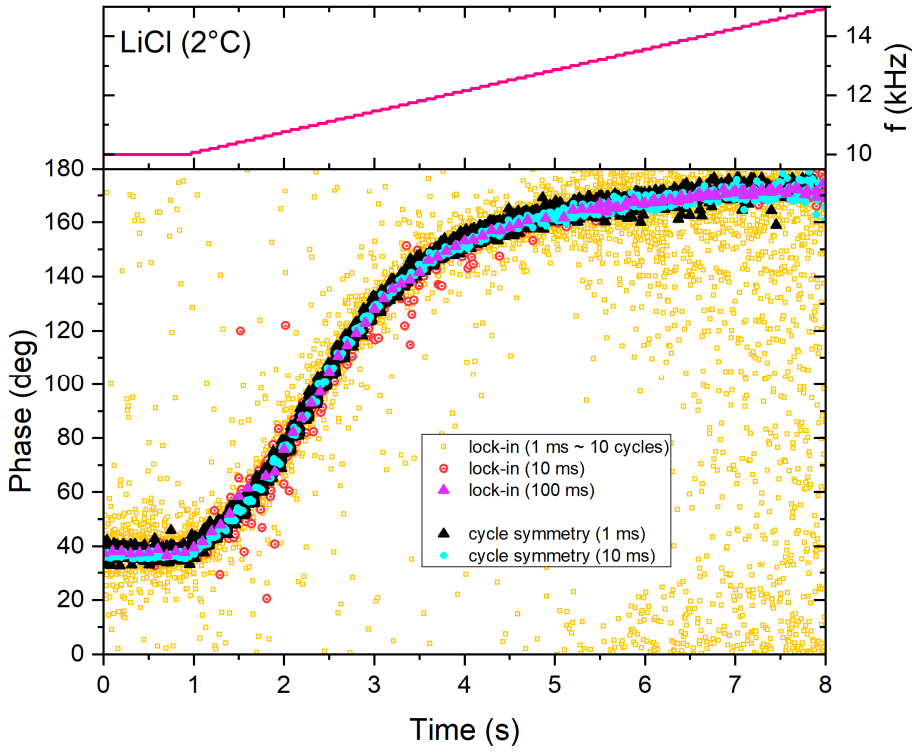

Figure S10 *Comparison of phase shift analysis methods using the light scattered by an oscillating liquid droplet of LiCl solution (~0.3 mol L^{-1}) at T=2 °C. Top panel: reference frequency. Bottom panel: Phase shift determined using cycle symmetry and lock-in methods while applying a frequency sweep extending over the droplet's natural oscillation frequency (phase=90°).*

The data in Figure S10 is for a liquid droplet of LiCl solution. Depending on solute concentration and relative humidity in the EDB, water evaporates from the droplet. After the droplet attained equilibrium size, a frequency sweep was applied and the scattered light recorded. In this way size change during application of the frequency sweep was avoided which could potentially influence subsequent analysis. The frequency sweep and the result from the phase shift analysis using both methods are shown in Fig. S10. The comparison shows that with analysis of only a few cycles (1 ms=10 cycles @10 kHz), the cycle symmetry method shows a much lower variability in the resulting phase shift compared to the lock-in method. The variability of the latter reduces significantly when analysing longer portions of the output signal (10 ms=100 cycles @10 kHz). The variability improves even more when analysing 100ms portions.

6. High viscosity limit

To illustrate a potential limitation of the method at higher viscosity we computed the phase shift according to Eq. (5) from the manuscript for various values of the viscosity ranging from 2 mPa s to 1 Pa s. The result is shown in panel A of Fig. S11 for a droplet of R=50 µm, ρ=1000 kg m^{-3}, Q=0.8 pC, σ=0.07 N m^{-1}. For viscosity above a few Pa s the phase frequency curve becomes rather flat indicating that a high uncertainty in the fitted parameters can be expected. To provide an idea about the width of the resonance and the amplitude of oscillation, we also calculated the corresponding oscillation amplitude. The result is shown in panel B of Fig. S11. Here, all calculated curves are scaled in the vertical direction by an identical factor

which was determined by matching the 2mPas curve to data retrieved from a manual analysis of a single water droplet measurement at about 0 °C (~2 mPa s). The graph shows that the resonance peak disappears for viscosity above about 20 mPas and that the amplitude reduces even further posing an additional challenge for detecting the oscillations at higher viscosity.

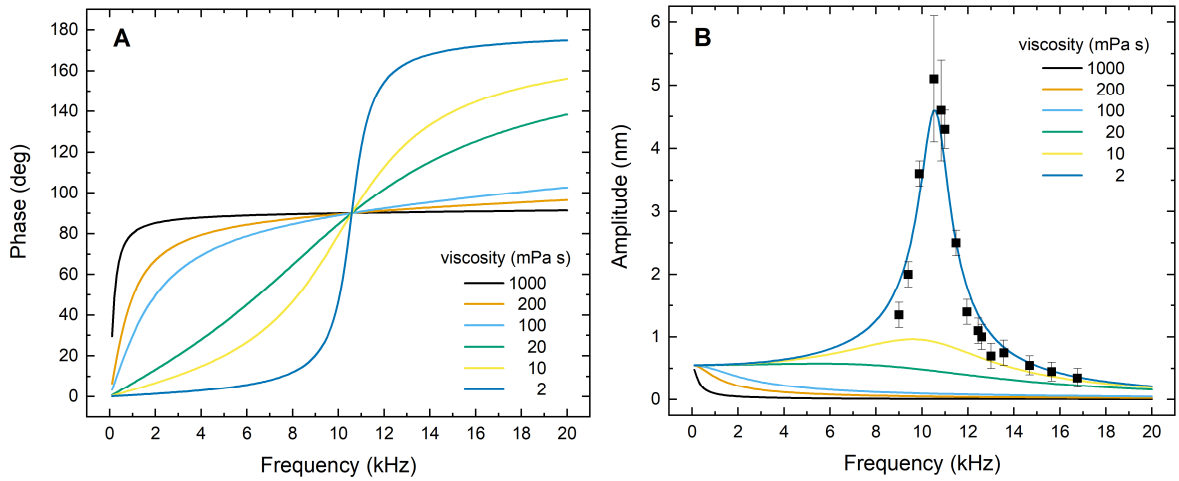

Figure S11 *Calculated phase shift and amplitude of oscillation for a water droplet as function of excitation frequency in the EDB for various viscosity values. The data points represent the results of oscillation amplitude analysis for a single water droplet at 0°C (~2 mPa s). More details are given in the text.*

Based on these considerations, we conclude that a viscosity above a few Pa s represents a current upper limit for this method.

References

Bohren, C. F. and Huffman, D. R.: Absorption and scattering of light by small particles, John Wiley & Sons, 2008.

Davies, J. F.: Mass, charge, and radius of droplets in a linear quadrupole electrodynamic balance, Aerosol Science and Technology, 53, 309-320, https://doi.org/10.1080/02786826.2018.1559921, 2019.

Duft, D.: Laborexperimente zur Mikrophysik der Wolken, Ph.D. thesis, Technical University Ilmenau, Germany, https://www.db-thueringen.de/receive/dbt_mods_00019099, 2011.

Steiner, B., Berge, B., Gausmann, R., Rohmann, J., and Rühl, E.: Fast in situ sizing technique for single levitated liquid aerosols, Appl. Opt., 38, 1523-1529, https://doi.org/10.1364/AO.38.001523, 1999.